Microchemical Journal 200 (2024) 110520

Contents lists available at ScienceDirect

Microchemical Journal

journal homepage: www.elsevier.com/locate/microc

Dansyl-modified tryptophan fluorescence sensor for highly sensitive and selective detection of Hg^{2+} in aqueous solutions

Lianshun Zhang [a], Peiran Zhao [b], Shuaibing Yu [a], Jinming Kong [c], Lei Gao [b,*], Lianzhi Li [a,*]

[a] School of Chemistry and Chemical Engineering, Liaocheng University, Liaocheng 252059, PR China
[b] Zhong Yuan Academy of Biological Medicine, Liaocheng People's Hospital, Liaocheng 252000, PR China
[c] School of Environmental and Biological Engineering, Nanjing University of Science and Technology, Nanjing, Jiangsu 210094, PR China

ARTICLE INFO

Keywords:
Dansylated tryptophan
Fluorescence sensor
Hg^{2+} detection
Turn-on response

ABSTRACT

A new fluorescent sensor of dansylated tryptophan (DW) was synthesized using solid phase peptide synthesis (SPPS). Upon the addition of different metal ions, only the presence of Hg^{2+} induced an increase in DW fluorescence intensity with a blue shift from 550 to 496 nm. DW was highly sensitive and selective for detecting Hg^{2+} with a low detection limit of 6.53 nM in 20 mM HEPES buffer (pH 7.4). The turn-on response could be attributed to the combination of chelation enhanced fluorescence (CHEF) and solvatochromic effects. The binding constant of DW with Hg^{2+} ion was determined to be 9.4×10^4 $M^{-1/2}$ with a stoichiometric ratio of 2: 1. The DW + Hg^{2+} complex can be reversed with EDTA and reused with excellent circulation effect. The fluorescence lifetime and absolute quantum yield of DW were studied before and after the addition of Hg^{2+}. Further characterizations of the interaction between DW and Hg^{2+} were conducted by IR and NMR.

1. Introduction

Amino acids are the simplest biological structural units, and they have good biocompatibility [1,2]. However, with the exception of tryptophan, phenylalanine, and tyrosine [3,4], natural amino acids generally do not exhibit fluorescence properties. Concurrently, certain amino acids can serve as active sites for toxic metals [5]. On the other hand, dansyl fluorophore has been extensively utilized in fluorescent sensors for the detection of metal ions specific to sulfonamide groups. Furthermore, the internal charge transfer (ICT) effect that involves dimethylamino and sulfonamide makes the dansyl moiety sensitive to its surrounding microenvironment and specific metal ions. The detection of toxic metal ions in aquatic ecosystems has always been an important topic. Mercury is known as one of the most common and toxic elements [6]. The toxicity of Hg^{2+} to organisms is mainly due to its ability to combine with sulfhydryl groups in enzymes and proteins, resulting in their inactivation and loss of function. This can eventually lead to some diseases, such as heart disease and renal failure. Mercury ions are widespread in the environment and can be enriched in the human body, posing a significant threat to human health [7–10]. Therefore, it is increasingly important to find a method for detecting Hg^{2+} with a low detection limit, high sensitivity, simple detection and recyclability. Currently, traditional methods for detecting Hg^{2+} include atomic absorption spectroscopy (AAS) [11], atomic emission spectroscopy (AES) [12] and inductively coupled plasma mass spectrometry (ICP-MS) [13]. Nevertheless, these methods frequently necessitate the use of costly instrumentation, involve intricate sample preparations, employ tedious detection processes and require specialized operational techniques.

Compared with traditional techniques, sensors based on fluorescent measurements have received much attention for detecting toxic metal ions. Currently, many fluorescence sensors for detecting Hg^{2+} have been developed, such as carbon dots (CDs), DNA enzymes, nanoparticles and proteins [14–17]. Nevertheless, these fluorescence sensors have some disadvantages, including complicated synthesis processes, poor solubility in water, and the need for a high proportion of organic solvents or long reaction time at high temperature. These limitations are a hindrance because Hg^{2+} is often present in biological and ecological environments of aqueous solutions. Therefore, it is becoming increasingly important to find a simple, fast, and recyclable sensor for Hg^{2+} detection in aqueous solutions [6,18]. In this paper, we designed and synthesized a new fluorescent sensor, dansyl-tryptophan (DW). The sensor displayed highly selective and sensitive detection of Hg^{2+} based on the chelation-enhanced fluorescence effect and solvatochromic effect in HEPES buffer [19].

* Corresponding authors at: No. 1, Hunan Road, Liaocheng 252059, PR China.
E-mail addresses: gaolei_0635@126.com (L. Gao), lilianzhi1963@163.com (L. Li).

https://doi.org/10.1016/j.microc.2024.110520
Received 21 August 2023; Received in revised form 20 March 2024; Accepted 9 April 2024
Available online 10 April 2024
0026-265X/© 2024 Elsevier B.V. All rights reserved.

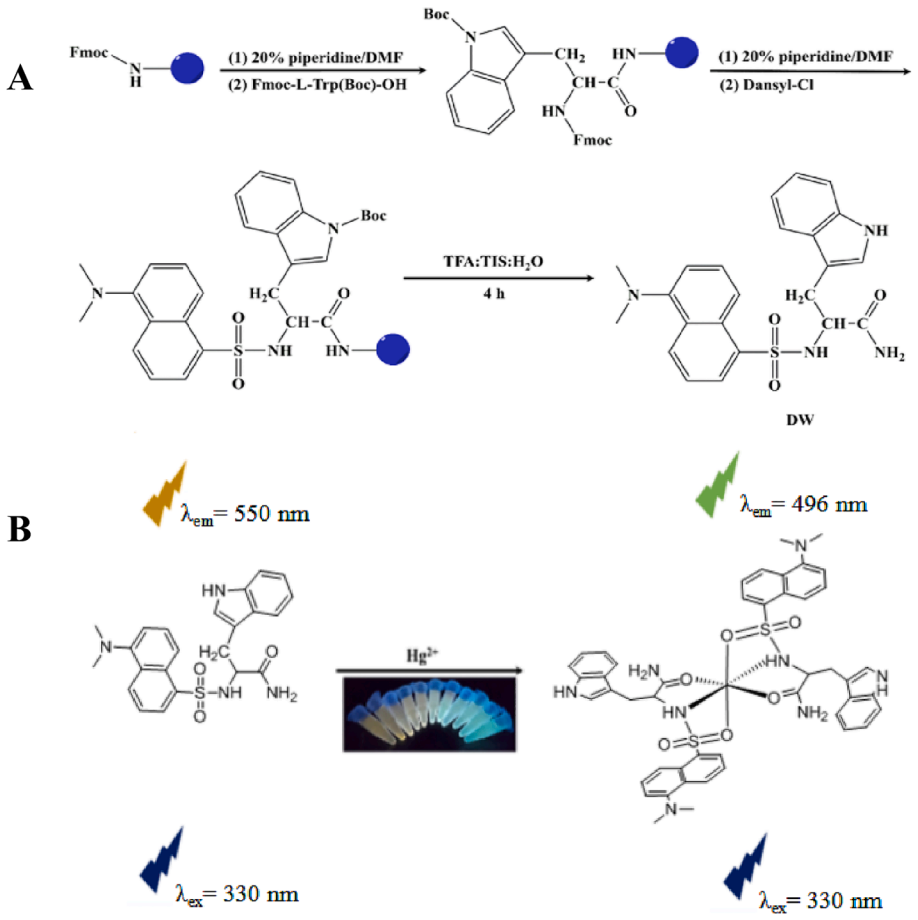

Scheme 1. (A) Solid phase synthesis scheme of the sensor DW. (B) The proposed principle of DW for detecting Hg^{2+} ion.

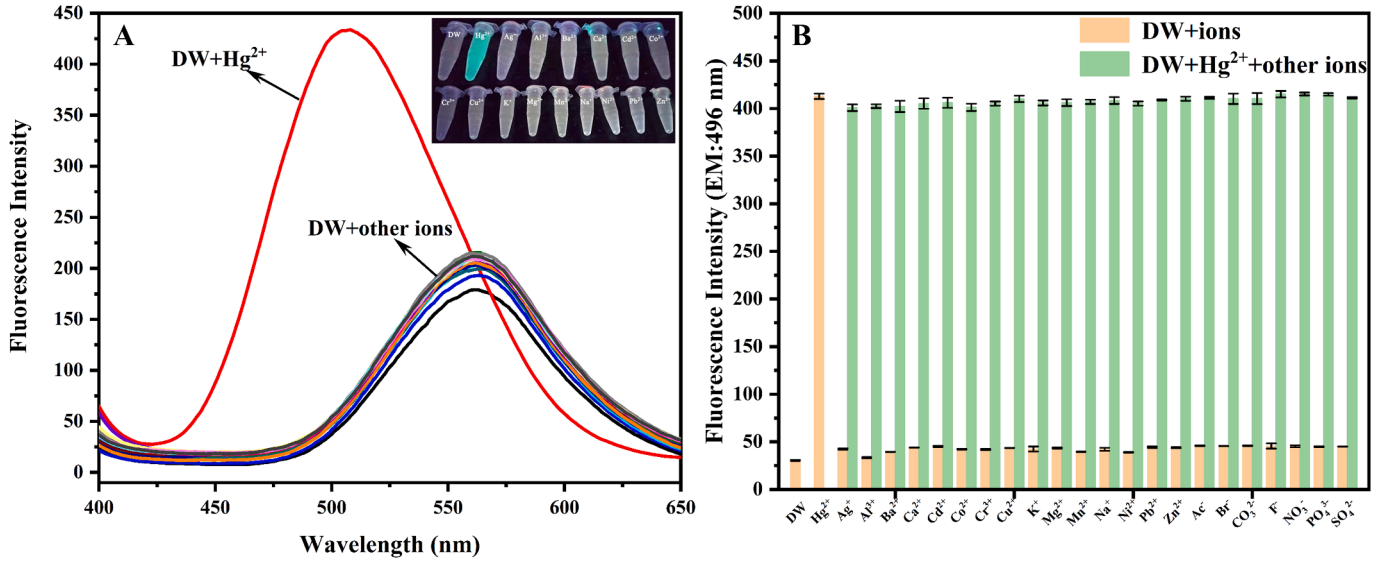

Fig. 1. (A) Fluorescence spectra of 20.0 μM DW in the presence of 16 metal ions and 7 anions (20.0 μM) with excitation wavelength of 330 nm in 20 mM HEPES buffer at pH 7.4. Inset picture in (A) is the color changes of the systems excited by a 365 nm UV lamp in the presence of different metal ions. (B) The yellow bars in the histogram represent the fluorescence intensity values of different ions added to the DW system. The green bars represent the subsequent addition of 20.0 μM Hg^{2+} to the above solutions.

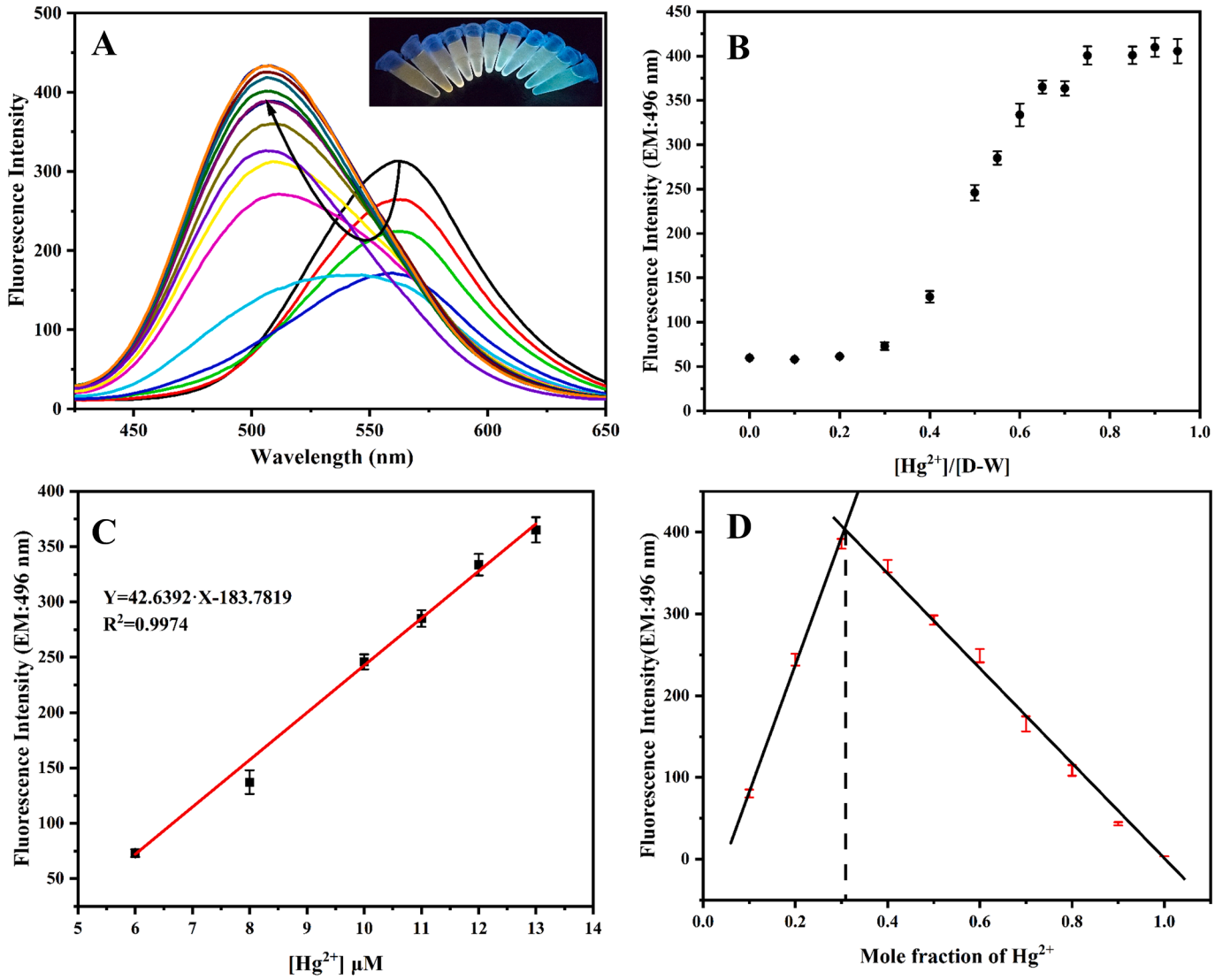

Fig. 2. (A) Fluorescence spectra of 20.0 μM DW with excitation wavelength of 330 nm upon addition of increasing concentrations of Hg^{2+} (0.0–20.0 μM) in 20 mM HEPES buffer at pH 7.4. Inset picture in (A) is the color changes of the systems excited by a 365 nm UV lamp. (B) Plot of the fluorescence intensity of DW as a function of concentration ratio of $[Hg^{2+}]/[DW]$ (C) Linear relationship of fluorescence intensity at 496 nm with increased concentration of Hg^{2+} in 20 mM HEPES buffer at pH 7.4. (D) Job's plot for DW with Hg^{2+} in 20 mM HEPES buffer at pH 7.4.

2. Experimental

2.1. Reagents and instruments

The details of the reagents and apparatus are given in the Supplementary Information.

2.2. Preparation of the sensor DW

DW was synthesized using a CS136 peptide synthesizer (Scheme 1). The details of the experimental steps are listed in the Supplementary Information. The HRMS of DW was analyzed in the positive ion mode (Fig. S1). The HRMS was calculated as 437.2 [DW + H^+]. Observed 437.3510 as [DW + H^+] and 261.1751 as [DW + HCOOH + K^++H^+].

^{1}H NMR (500 MHz, DMSO-d_6) δ 10.91 (d, J = 2.5 Hz, 1H), 8.76 (d, J = 8.5 Hz, 1H), 8.10 (d, J = 8.6 Hz, 1H), 8.03 (d, J = 5.6 Hz, 3H), 7.96 – 7.92 (m, 1H), 7.58 (d, J = 9.5 Hz, 1H), 7.52 – 7.45 (m, 2H), 7.44 (d, J = 7.9 Hz, 1H), 7.26 (d, J = 8.0 Hz, 1H), 7.10 (d, J = 2.4 Hz, 1H), 6.98 (ddd, J = 8.1, 6.9, 1.1 Hz, 1H), 6.92 – 6.87 (m, 1H), 4.05 (dt, J = 11.5, 5.8 Hz, 1H), 3.13 (d, J = 9.4 Hz, 2H), 3.06 (s, 6H) (Fig. S2). ^{13}C NMR (126 MHz, DMSO-d_6) δ 173.1, 137.0, 136.3, 129.4, 129.3, 129.2, 128.4, 127.9, 127.5, 124.5, 123.8, 121.2, 120.3, 118.6, 117.2, 115.7, 114.8, 111.6, 109.6, 57.3, 45.6, 29.1 (Fig. S3).

2.3. Fluorescence measurements

A stock solution of 1.3 mM DW was prepared in 20 mM HEPES buffer solution (pH 7.4) and stored at 4 °C. For all spectral measurements, appropriate dilutions were made using the same stock solution. Fluorescence spectra were measured in the range from 400 nm to 650 nm at an excitation wavelength of 330 nm [20]. Both excitation and emission slits were set at 5 nm. Fluorescence spectra of DW were recorded in the absence and presence of 16 metal ions (Hg^{2+}, Al^{3+}, Ba^{2+}, Ca^{2+}, Cd^{2+}, Co^{2+}, Cr^{3+}, Cu^{2+}, K^+, Mg^{2+}, Mn^{2+}, Na^+, Ni^{2+}, Pb^{2+} and Zn^{2+} as chloride salts, and Ag^+ as a nitrate salt) and 7 anions ($NaNO_3$, Na_2SO_4, Na_3PO_4, Na_2CO_3, NaAc, KF, and KBr) in 20 mM HEPES buffer solution at pH 7.4. All solutions were prepared immediately before use. Additionally, the binding reversibility of DW to Hg^{2+} was investigated by adding excess EDTA to the DW + Hg^{2+} system [21,22].

The fluorescence lifetime and fluorescence absolute quantum yields

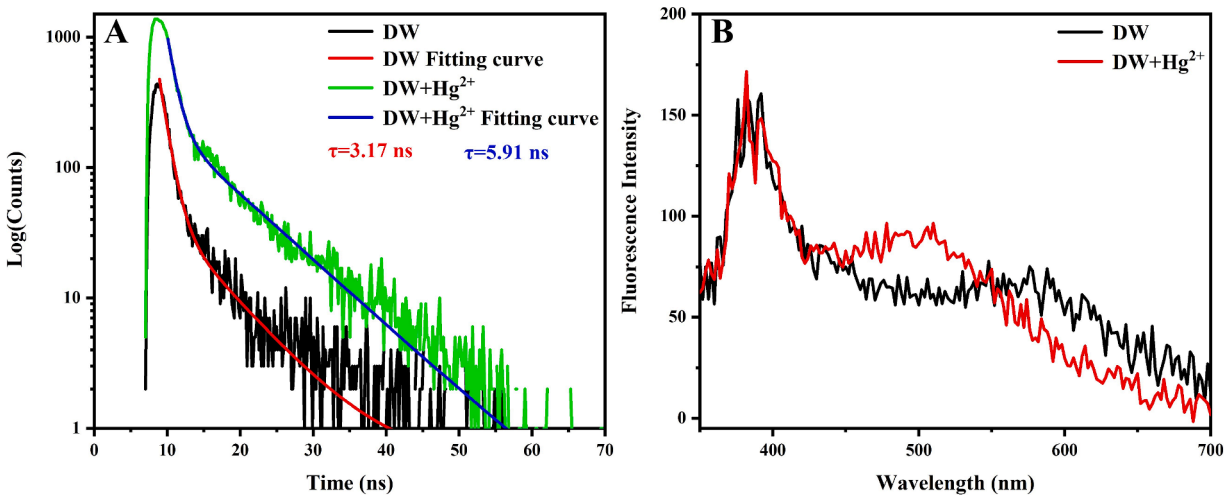

Fig. 3. (A) Fluorescence lifetime decay profiles excited at 330 nm for DW (10.0 μM) and DW + Hg^{2+} (10.0 μM) in 20 mM HEPES buffer (pH 7.4) at 496 nm emission. (B) 10 μM DW and 10 μM DW + Hg^{2+} fluorescence quantum yields.

Table 1
Summary of fluorescence lifetime measurements and quantum yield (QYs) in HEPES solution.

Sample	λ_{ex}	λ_{em}	τ[ns] (contribution, %)	χ^2	QYs
DW	330 nm	496 nm	$\tau_1 = 1.1072$ (64.01) $\tau_2 = 6.8514$ (35.99) $\tau = 3.17$	1.005	6.31 %
DW + Hg^{2+}	330 nm	496 nm	$\tau_1 = 1.1160$ (36.32) $\tau_2 = 8.6366$ (63.68) $\tau = 5.91$	1.065	10.41 %

were measured using an FLS 1000 Photoluminescence Spectrometer (UK). The fitting of fluorescence lifetime was carried out according to the following formula: $R(t) = B_1e^{(-t/\tau 1)} + B_2e^{(-t/\tau 2)}$; $R(t) = B_1e^{(-t/\tau 1)} + B_2e^{(-t/\tau 2)} + B_3e^{(-t/\tau 3)}$. The fluorescence lifetime was obtained by $[\tau] = \Sigma\tau_iB_i$. The quality of the fit could be determined by the χ^2 value [23–26].

2.4. Determination of the binding constant of DW with Hg^{2+}

The binding constant between DW and Hg^{2+} was calculated by the modified Benesi-Hildebrand equation: $\Delta FI_{max}/\Delta FI = 1 + M^{-n}/K$, where $\Delta FI_{max} = FI_{max} - FI_0$ and $\Delta FI = FI_x -$, FI_{max} is the maximum fluorescence intensity of DW in the state of complete Hg^{2+} binding, FI_0 is the fluorescence intensity of DW and FI_x is the fluorescence intensity of DW at various Hg^{2+} concentrations. [M] presents the Hg^{2+}concentration, and n is the binding number of Hg^{2+} ion to each DW molecule (here $n = 1/2$), while K is the binding constant [27,28].

3. Results and discussion

3.1. DW selectivity for Hg^{2+} and interference from other ions

The fluorescence responses of DW (20.0 μM) to 16 metal ions (Hg^{2+}, Al^{3+}, Ba^{2+}, Ca^{2+}, Cd^{2+}, Co^{2+}, Cr^{3+}, Cu^{2+}, K^+, Mg^{2+}, Mn^{2+}, Na^+, Ni^{2+}, Pb^{2+} and Zn^{2+} as chloride salts, and Ag^+ as a nitrate salt) (20.0 μM) and 7 anions ($NaNO_3$, Na_2SO_4, Na_3PO_4, Na_2CO_3, NaAc, KF, and KBr) (20.0 μM) were measured in 20.0 mM HEPES buffer (pH 7.4). As shown in Fig. 1A, among the various metal ions, only Hg^{2+} showed a strong fluorescence-enhanced response along with a 54 nm blueshift from 550 nm to 496 nm (yellow to green). The observed fluorescence enhancement and blueshift effect may be due to the chelation-enhanced fluorescence (CHEF) effect and the solvatochromic effect [29]. The close-packed indole and dansyl moieties partially shielded the dansyl group from the solvent and increased its hydrophobic environment. In the inset of Fig. 1A, the DW solution showed a yellow colour under a 365 nm UV lamp, while the addition of Hg^{2+} caused the colour to turn green. The DW solution containing other mixed-metal ions still retained the yellow colour. The interference of other ions with DW fluorescence in the presence of Hg^{2+} was studied. As shown in Fig. 1B, it was observed that other ions had little effect on the fluorescence intensity of DW-Hg^{2+} and remained green, demonstrating its ability to detect Hg^{2+}.

3.2. Detection limit and binding mechanism study of DW with Hg^{2+}

First, the fluorescence spectra of 20 μM DW were measured at different concentrations of Hg^{2+} in a 20 mM HEPES buffer (pH 7.4) at a 330 nm excitation wavelength. As shown in Fig. 2A, with the continuous addition of Hg^{2+}, the emission peak of the fluorescence spectra of DW gradually blueshifted. The maximum fluorescence emission peak shifted by 54 nm from 550 nm to 496 nm, and its fluorescence intensity exceeded that of DW itself at an excitation wavelength of 330 nm. From the inset of Fig. 2A, it can be seen that the addition of different concentrations of Hg^{2+} into the DW solution gradually changed the colour from yellow to green under irradiation with a 365 nm UV lamp. Fig. 2B shows the fluorescence intensities at 496 nm under different ratios of Hg^{2+} to DW. Fig. 2C shows the DW fluorescence titration of Hg^{2+} ion in the range from 6 μM to 13 μM, which exhibited a good linear relationship between the fluorescence intensity and Hg^{2+} concentration (R^2 = 0.9974). Then, the limit of detection (LOD) was calculated as $3\sigma/k$, where σ refers to the standard deviation of blank measurements, and k is the slope of the line. According to the equation, the detection limit of DW for Hg^{2+} was as low as 6.53 nM. Table S1 shows a comparison of the performance between this method and other methods reported previously. The high sensitivity of the DW sensor for fluorescence detection of Hg^{2+} makes this method a comparable, if not better, method than other reported approaches. This detection limit is within the safety level for drinking water stipulated by the World Health Organization (WHO). The binding stoichiometry of DW for Hg^{2+} was investigated by Job's plot method for the system (Fig. 2D). The result exhibited a maximum fluorescence intensity at 0.3 mol fraction for Hg^{2+} in a 20 mM HEPES buffer at DW concentrations from 20.0 μM to 0.0 μM. This result also suggests that DW formed approximately 2:1 complex with Hg^{2+} in the HEPES buffer.

3.3. UV and CD spectra of the DW-Metal ions system

As shown in Fig. S4, the UV spectral results showed that DW exhibits

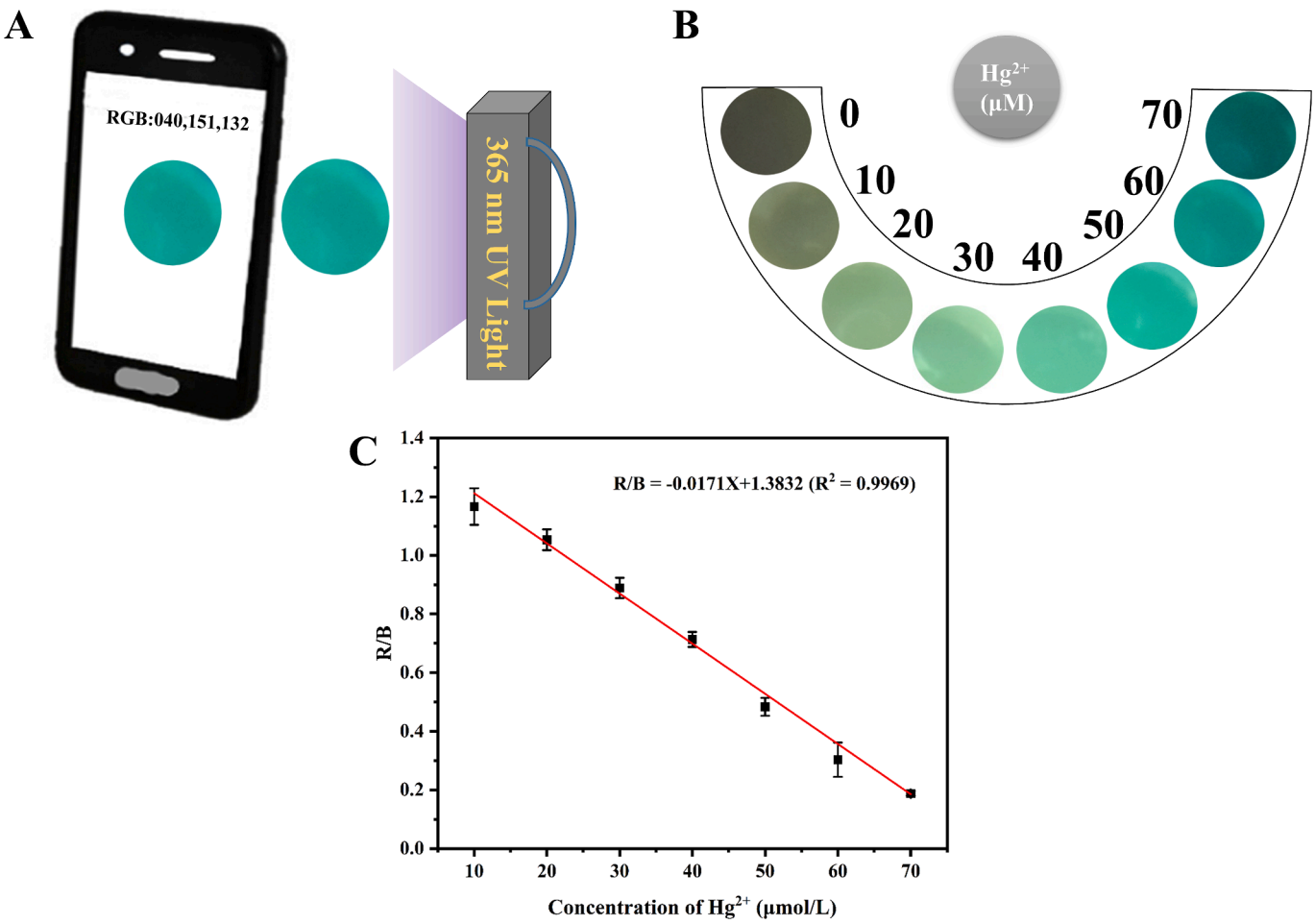

Fig. 4. (A) Schematic diagram of Hg^{2+} detection by a smartphone. (B) Circular gel sheet of DW in agarose for visual recognition of Hg^{2+}. (C) The relationship between the colour change (R/B) of the circular gel sheet and the Hg^{2+}concentration.

Table 2
Detection of Hg^{2+} in tap water.

Water sample	Hg^{2+} added (μM)	Hg^{2+} found (μM)	Recovery (%)
1	6.0	7.7 ± 0.74	128.3 ± 0.12
2	7.0	8.2 ± 0.42	117.1 ± 0.60
3	8.0	8.9 ± 0.41	111.2 ± 0.05
4	9.0	9.4 ± 0.29	104.4 ± 0.03
5	10.0	9.9 ± 1.82	99.0 ± 0.18

absorption peaks at 220 nm, 250 nm, 285 nm (tryptophan residue), and 330 nm (Dansyl), respectively. In the presence of 16 metal ions, where the addition of Hg^{2+} leads to an obvious decrease at 220 nm in the DW spectra. The result indicated that DW may be chelated with Hg^{2+} via the sulfonamide group of the dansyl fluorescent moiety and the side chain group of the amino acid residues.

However, except for 220 nm, the change of absorption of other wavelengths is small, so it is difficult to act as a sensor to detect Hg^{2+} by UV–Vis spectra. Furthermore, the visible area is not absorbed.

Next, we analysed the circular dichroism (CD) spectra of DW alone and with added metal ions. As shown in Fig. S5, the CD spectrum of DW (50 μM) displayed a positive peak at 233 nm and a negative peak at 248 nm. Among the 16 tested metal ions, the positive and negative peaks of the CD spectra were significantly reduced only when Hg^{2+} was added. As the concentration of Hg^{2+} increased from 0 to 50 μM, the two peaks gradually decreased until the Hg^{2+} concentration reached 25 μM. After this point, the signal no longer changed regularly, and the curve remained stable (Fig. S6). This observation indicated that DW interacted specifically with Hg^{2+}.

Second, the binding constant of Hg^{2+} to DW calculated by the modified Benesi-Hildebrand equation was 9.6×10^4 $M^{-1/2}$ (R^2 = 0.9935) (Fig. S7), indicating that DW had a strong binding affinity to Hg^{2+}.

Additionally, the fluorescence lifetime and absolute quantum yields (QYs) of DW and DW + Hg^{2+} solutions were further examined. As shown in Fig. 3A, the fluorescence lifetime decay profiles of DW and DW + Hg^{2+} solutions revealed that the fluorescence lifetime of DW was 3.17 ns at 550 nm emission, and it increased to 5.91 ns after the combination of DW and Hg^{2+}. The results of the fluorescence lifetime measurements are presented in Table 1. Moreover, as shown in Fig. 3B, the QYs of DW and DW + Hg^{2+} were determined, and it was observed that the QYs of DW and DW + Hg^{2+} were 6.31 % and 10.41 %, respectively (Table 1). These findings indicated that the QY of DW + Hg^{2+} was higher than that of DW. It is worth noting that the fluorescence intensity, fluorescence lifetime, and QYs of DW + Hg^{2+} were all enhanced compared with those of DW alone. This serves as evidence for the CHEF effect between Hg^{2+} and DW.

3.4. Application of DW for detecting Hg^{2+}

To enable accurate visual detection of Hg^{2+} ion, DW was dissolved in agarose solution to create a circular gel sheet. The agarose gel flakes were then immersed in aqueous solutions of varying Hg^{2+} concentrations and left for 30 min. The colours of the resulting gel flakes were observed using a 365 nm UV lamp, as depicted in Fig. 4. We used a smartphone to capture pictures of the colour change process and read

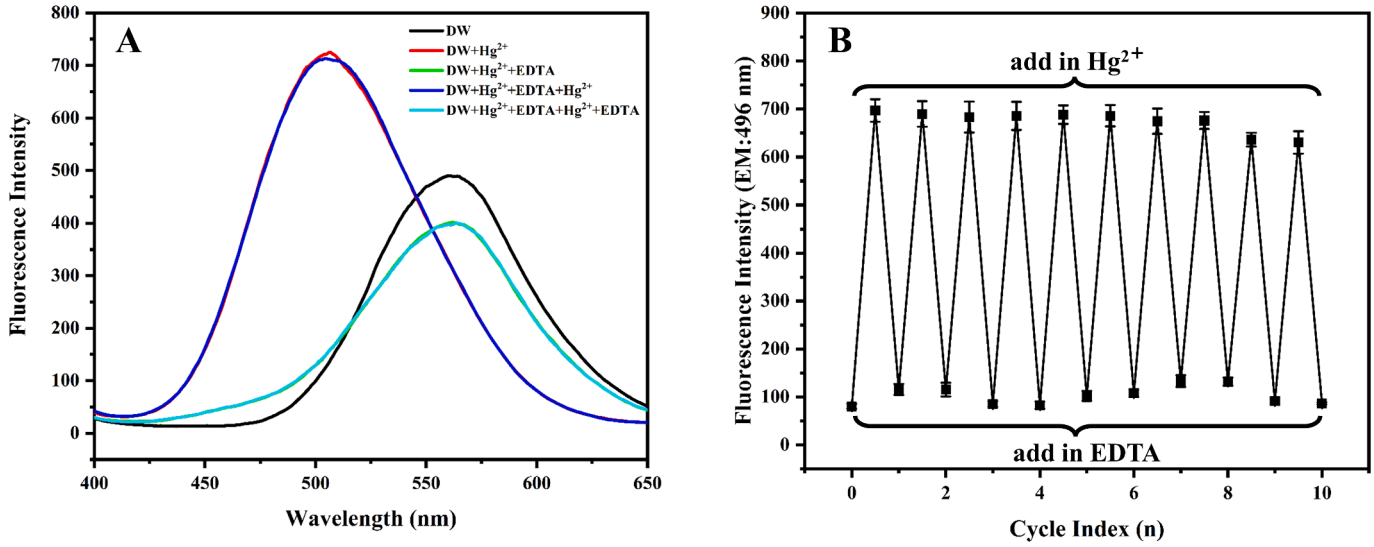

Fig. 5. (A) The fluorescence spectra for reversibility experiment of DW toward Hg^{2+} by adding EDTA in 20.0 mM HEPES buffer (pH 7.4). (B) The cycle index of DW-Hg (30.0 μM) reacting with EDTA (2.0 equiv). Emission wavelength: 496 nm.

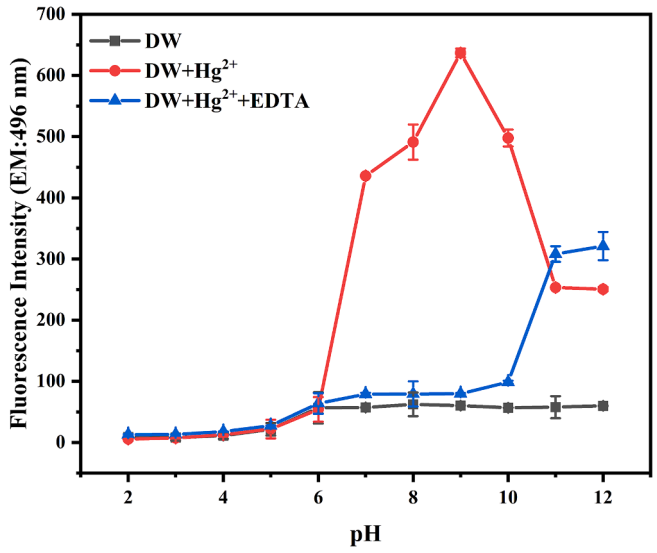

Fig. 6. The pH effect on the fluorescence intensity of 20.0 μM DW (black line) and in the presence of 1.0 equiv Hg^{2+} (red line) and 2.0 equiv EDTA (blue line).

the RGB values using a colour recognition APP (Fig. 4A). The RGB ratio (R/B) corresponding to the red and blue channels was plotted against the Hg^{2+} concentration. We found that the fluorescent green colour deepened gradually as the concentration of Hg^{2+} increased from 0 to 70 μM. In the gel sheet system, the R/B value and Hg^{2+} concentration showed a good linear relationship in the range of 10–70 μM. The corresponding linear regression equation was R/B = –0.0171X + 1.3832 (R^2 = 0.9969).

In addition, in order to further study the application of DW in real water sample detection, the sensor was used to detect Hg^{2+} in tap water. The fluorescence titration curve was used as a standard curve and then recovery was achieved by adding Hg^{2+} to the tap water sample. As shown in Table 2, the DW sensor has good recoveries for Hg^{2+} in the range of 6–10 μM, indicating its potential for monitoring Hg^{2+} in real water samples.

3.5. *Recycling test of DW to Hg^{2+} by EDTA and effect of pH*

To better understand the reversibility of the interaction between DW and Hg^{2+}, we performed an EDTA reversible experiment. Our results showed that when 30 μM DW and 30 μM Hg^{2+} reacted to form a chelation complex, green fluorescence was generated. However, upon the addition of 2.0 equiv EDTA, which acts as a chelator, the interaction between Hg^{2+} ion and DW was reversed, leading to a change in fluorescence from green to yellow. Additionally, cycle experiments demonstrated that the detection of Hg^{2+} ion by DW was reversible and could be cycled up to 10 times (Fig. 5). Therefore, the fluorescence property of DW can be used for repeating "off-on-off" switching as needed.

The influences of pH on the DW, DW + Hg^{2+} and DW + Hg^{2+}+EDTA systems were measured. Fig. 6 shows that at acidic pH levels (pH < 6), both DW and DW + Hg^{2+} exhibited weak fluorescence intensities, rendering the detection of Hg^{2+} impossible. However, at alkaline pH levels (pH 7 ~ 12), the fluorescence intensities of DW and DW + Hg^{2+} were significantly different, and the fluorescence intensity of DW + Hg^{2+} appeared to be the maximum in the pH 9 solution in which the formation of the DW + Hg^{2+} complex was conducive. Therefore, DW is an effective sensor for monitoring Hg^{2+} in neutral or alkaline environments. When 2.0 equiv of EDTA was added to the DW + Hg^{2+} solution at different pH values, its fluorescence intensity was almost constant at pH 2–10, but it was ineffective when pH > 11.

To further study the effects of pH on fluorescence of DW + Hg^{2+}, as shown in Fig. S8, DW and DW + Hg^{2+} were separately irradiated at different pH solutions under a 365 nm UV lamp, the results were consistent with the above spectral measurements.

3.6. *Characterization of DW and DW + Hg^{2+}*

IR spectroscopy was used to identify the chemical groups of DW that interacted with Hg^{2+}, as shown in Fig. S9. Peaks at 3424.6 cm^{-1} and 3286.7 cm^{-1} indicate the stretching vibrations of NH_2 and N-H in DW, respectively [30]. The peak at 3128.0 cm^{-1} represents the stretching vibration of Ar-H. The peaks at 1871.6 cm^{-1} and 1384.9 cm^{-1} correspond to the stretching vibration and asymmetric vibration of the O═S═O covalent group [31,32]. The stretching vibration peaks of the amide bond are observed at 1693.9 cm^{-1} and 1654.0 cm^{-1} [20]. The bands of C—N, C—S stretching vibrations, and C—H deformation are displayed between 1454.3–1102.5 cm^{-1}. The disappearance of the

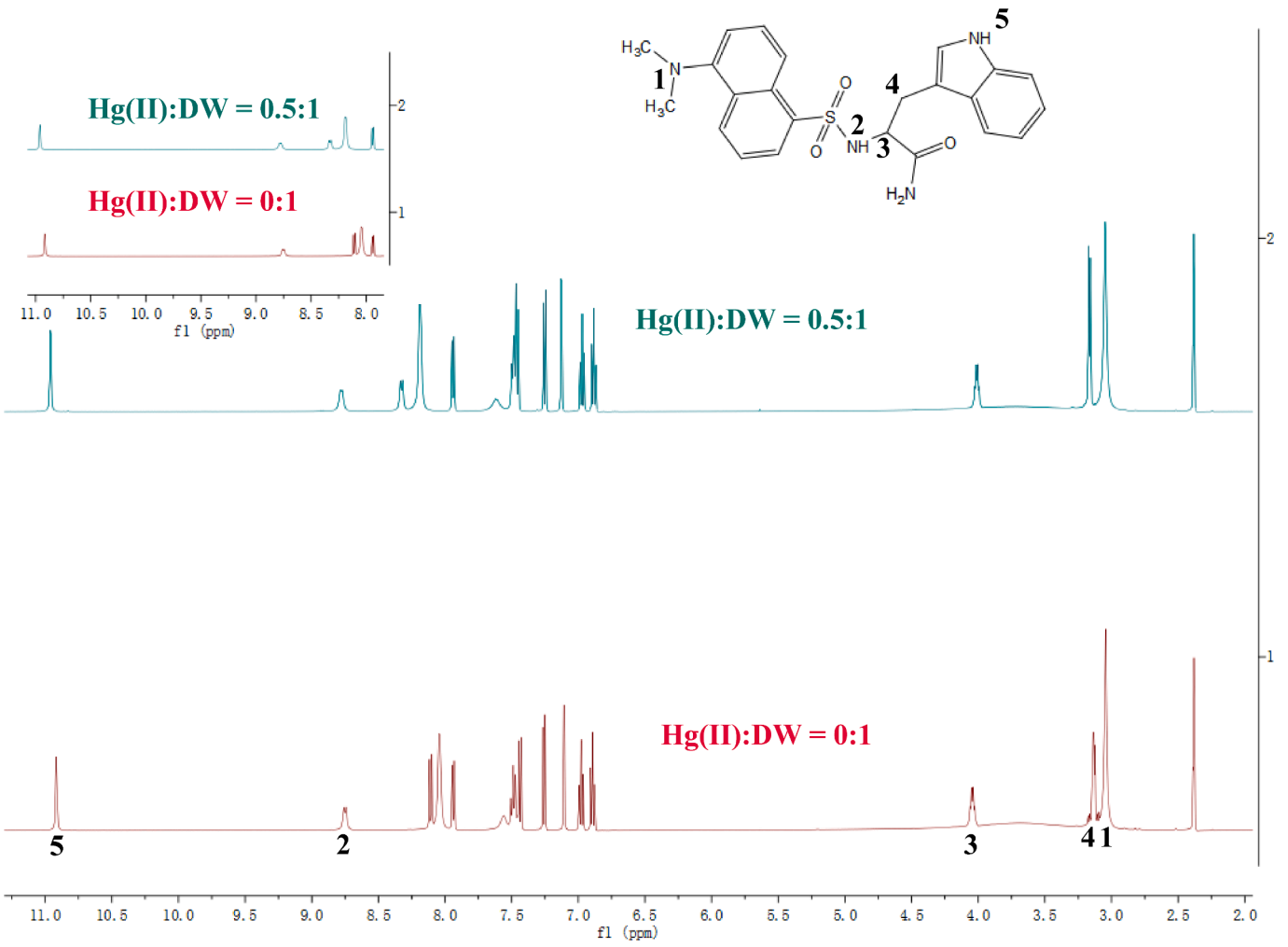

Fig. 7. ^{1}H NMR titration spectra of 50.0 mM DW in the absence and presence of Hg^{2+} (0.5, 1.0 equiv).

stretching vibration of the N-H and O═S═O peaks, as well as the decrease in the stretch vibration peak of the amide bond, in the presence of Hg^{2+} suggest the involvement of these chemical groups in the interaction with Hg^{2+}.

^{1}H NMR experiments were conducted to determine binding sites in the interaction between DW and Hg^{2+}, as depicted in Fig. 7. The addition of Hg^{2+} caused a downfield chemical shift in imino H(2) linked to the dansyl group, indicating involvement in the coordination to Hg^{2+}. Additionally, the H in the benzene ring region changed slightly, potentially due to environmental changes after coordination of DW to Hg^{2+}.

3.7. Density functional theory investigation

All data in this study were calculated with the Gaussian 16 software package [33], and were optimized at the B3LYP level of density functional theory (DFT) [34]. The basis set 6-31G was selected for all non-metal atoms and lanl2dz for Hg^{2+}. Vibrational frequency analysis was computed to ensure the points that the minimum have no imaginary frequency. All the energetic values reported in this work are Gibbs free energies at 298.15 K. The calculation results are shown in Fig. 8. The binding of the two molecules DW and Hg^{2+} reduces the Gibbs free energy by 325.0 kcal/mol, indicating that the reaction is easy to proceed.

4. Conclusions

We have synthesized a highly selective, sensitive and effective sensor for Hg^{2+}, dansyl-modified tryptophan (DW). DW exhibited a fluorescence turn-on response to Hg^{2+} in 20 mM HEPES buffer with a low detection limit based on the CHEF effect and solvatochromic effect. The fluorescence lifetime of the sensor changed from 3.17 ns to 5.91 ns before and after the addition of Hg^{2+} at an excitation wavelength of 330 nm and an emission wavelength of 550 nm. The QYs increased from 6.31 % to 10.41 % after the addition of Hg^{2+}. Moreover, DW exhibited reversible behaviour for Hg^{2+} detection in the presence of EDTA. The study could provide a new method for developing low-cost and sensitive sensors for Hg^{2+} detections in both biological and environmental applications.

CRediT authorship contribution statement

Lianshun Zhang: Writing – original draft, Methodology, Investigation, Data curation, Conceptualization. **Peiran Zhao:** Investigation. **Shuaibing Yu:** Investigation. **Jinming Kong:** Supervision, Funding acquisition. **Lei Gao:** Writing – review & editing, Investigation, Formal analysis. **Lianzhi Li:** Writing – review & editing, Supervision, Funding acquisition, Conceptualization.

Declaration of competing interest

The authors declare that they have no known competing financial interests or personal relationships that could have appeared to influence the work reported in this paper.

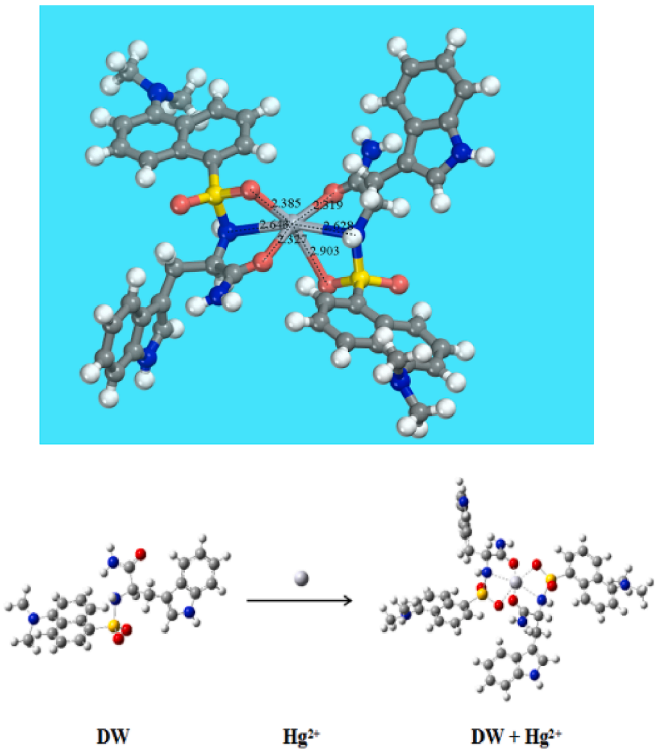

Fig. 8. DFT calculation for the binding of DW with Hg^{2+}.

Data availability

Data will be made available on request.

Acknowledgements

This work was supported by the Scientific Research Foundation of Liaocheng University, China (No. 318011919), and the National Natural Science Foundation of China (No. 21974068).

Appendix A. Supplementary data

Supplementary data to this article can be found online at https://doi.org/10.1016/j.microc.2024.110520.

References

[1] P. Chakraborty, E. Gazit, Amino acid based self-assembled nanostructures: complex Structures from remarkably simple building blocks, Nano. Mat. 4 (2018) 730–740, https://doi.org/10.1002/cnma.201800147.
[2] M. Wang, M. Zhou, L. Zhang, Z. Zhang, W. Zhang, A step-economic and one-pot access to chiral C(α)-tetrasubstituted α-amino acid derivatives via a bicyclic imidazole-catalyzed direct enantioselective C-acylation, Chem. Sci. 11 (2020) 4801–4807, https://doi.org/10.1039/D0SC00808G.
[3] L. Jørgensen, C.A. Stedmon, T. Kragh, S. Markager, M. Middelboe, M. Søndergaard, Global trends in the fluorescence characteristics and distribution of marine dissolved organic matter, Mar. Chem. 126 (2011) 139–148, https://doi.org/10.1016/j.marchem. 2011.05.002.
[4] P.R. Callis, Binding phenomena and fluorescence quenching. II: Photophysics of aromatic residues and dependence of fluorescence spectra on protein conformation, J. Mol. Struct. 1077 (2014) 22–29, https://doi.org/10.1016/j.molstruc.2014.04.051.
[5] M. Vandenbossche, M. Jimenez, M. Casetta, M. Traisnel, Remediation of heavy metals by biomolecules: A review, Crit. Rev. Environ. Sci. Technol. 45 (2015) 1644–1704, https://doi.org/10.1080/10643389.2014.966425.
[6] A. Aliberti, P. Vaiano, A. Caporale, M. Consales, M. Ruvo, A. Cusano, Fluorescent chemosensors for Hg^{2+} detection in aqueous environment, Sens. Actuators B 247 (2017) 727–735, https://doi.org/10.1016/j.snb.2017.03.026.
[7] P. Olmedo, A. Pla, A.F. Hernández, F. Barbier, L. Ayouni, F. Gil, Determination of toxic elements (mercury, cadmium, lead, tin and arsenic) in fish and shellfish samples. Risk assessment for the consumers, Environ. Int. 59 (2013) 63-72, https://doi.org/10.1016/j. envint.2013.05.005.
[8] X. Wu, S.J. Cobbina, G. Mao, H. Xu, Z. Zhang, L. Yang, A review of toxicity and mechanisms of individual and mixtures of heavy metals in the environment, Environ. Sci. Pollut Res. 23 (2016) 8244–8259, https://doi.org/10.1007/s11356-016-6333-x.
[9] X.F. Hu, M. Lowe, H.M. Chan, Mercury exposure, cardiovascular disease, and mortality: A systematic review and dose-response meta-analysis, Environ. Res. 193 (2021) 110538, https://doi.org/10.1016/j.envres.2020.110538.
[10] Y. Liu, Y. Deng, H. Dong, K. Liu, N. He, Progress on sensors based on nanomaterials for rapid detection of heavy metal ions, Sci. China. Chem. 60 (2017) 329–337, https://doi.org/10.1007/s11426-016-0253-2.
[11] S. Gupta, P. Pandotra, A.P. Gupta, J.K. Dhar, G. Sharma, G. Ram, M.K. Husain, Y.S. Bedi, Volatile (As and Hg) and non-volatile (Pb and Cd) toxic heavy metals analysis in rhizome of Zingiber officinale collected from different locations of North Western Himalayas by atomic absorption spectroscopy, Food Chem. Toxicol. 48 (2010) 2966-2971, https://doi.org /10.1016/j.fct.2010.07.034.
[12] R., Shekhar Improvement of sensitivity of electrolyte cathode discharge atomic emission spectrometry (ELCAD-AES) for mercury using acetic acid medium, Talanta 93 (2012) 32–36, https://doi.org/10.1016/j.talanta.2012.02.004.
[13] C.D.B. Amaral, R.S. Amais, L.L. Fialho, D. Schiavo, T. Amorim, A.R.A. Nogueira, F. R.P. Rocha, J.A. Nobrega, A novel strategy to determine As, Cr, Hg and v in drinking water by ICP-MS/MS, Anal. Methods 7 (2015) 1215–1220, https://doi.org/10.1039/C4AY02811B.
[14] D. Sun, T. Liu, C. Wang, L. Yang, S. Yang, K. Zhuo, Hydrothermal synthesis of fluorescent carbon dots from gardenia fruit for sensitive on-off-on detection of Hg^{2+} and cysteine, Spectrochim. Acta Part A 240 (2020) 118598, https://doi.org/10.1016 /j.saa.2020.118598.
[15] J. Huang, X. Gao, J. Jia, J.K. Kim, Z. Li, Graphene oxide-based amplified fluorescent biosensor for Hg^{2+} detection through hybridization chain reactions, Anal. Chem. 86 (2014) 3209–3215, https://doi.org/10.1021/ac500192r.
[16] H. Khani, S. Abbasi, Y.M. Tavakkoli, Y.N. Tan, A naked-eye colorimetric assay for detection of Hg^{2+} ions in real water samples based on gold nanoparticles-catalyzed clock reaction, J. Mol. Liq. 345 (2022) 118243, https://doi.org/10.1016/j.molliq.2021.118243.
[17] R. Wang, X. Zhou, H. Shi, Y. Luo, T-T mismatch-driven biosensor using triple functional DNA-protein conjugates for facile detection of Hg^{2}+, Biosens. Bioelectron. 78 (2016) 418–422, https://doi.org/10.1016/j.bios.2015.11.082.
[18] P. Wang, Y. An, J. Wu, Highly sensitive turn-on detection of mercury(II) in aqueous solutions and live cells with a chemosensor based on tyrosine, Spectrochim, Acta Part A 230 (2020) 118004, https://doi.org/10.1016/j.saa.2019.118004.
[19] G. Donadio, R. Di Martino, R. Oliva, L. Petraccone, P. Del Vecchio, B. Di Luccia, E. Ricca, R. Isticato, A. Di Donato, E. Notomista, A new peptide-based fluorescent probe selective for zinc(II) and copper(II), J. Mater. Chem. B 4 (2016) 6979–6988, https://doi.org/10.1039/C6TB00671J.
[20] X. Pang, J. Dong, L. Gao, L. Wang, S. Yu, J. Kong, L. Li, Dansyl-peptide dual-functional fluorescent chemosensor for Hg^{2+} and biothiols, Dyes Pigm. 173 (2020) 107888, https://doi.org/10.1016/j.dyepig.2019.107888.
[21] J. Fan, C. Chen, Q. Lin, N. Fu, A fluorescent probe for the dual-channel detection of Hg^{2+}/Ag^{+} and its Hg^{2+}-based complex for detection of mercapto biomolecules with a tunable measuring range, Sens. Actuators B 173 (2012) 874-881, https://doi.org/10.1016 /j.snb.2012.08.004.
[22] N. Dey, A simple strategy for the visual detection and discrimination of Hg^{2+} and CH_3Hg^{+} species using fluorescent nanoaggregates, Dalton Trans. 50 (2021) 12563–12569, https://doi.org/10.1039/D1DT01455B.
[23] S. Yu, Y. Li, L. Gao, P. Zhao, L. Wang, L. Li, Y. Lin, A highly selective and sensitive Zn^{2+} fluorescent sensor based on zinc finger-like peptide and its application in cell imaging, Spectrochim. Acta Part A 261 (2021) 120042, https://doi.org/10.1016 /j.saa.2021.120042.
[24] X. Zhao, Q. Tang, S. Zhu, W. Bu, M. Yang, X. Liu, M.Y. Meng, W. Yu, H. Sun, B. Yang, Controllable acidophilic dual-emission fluorescent carbonized polymer dots for selective imaging of bacteria, Nanoscale 11 (2019) 9526–9532, https://doi.org/10.1039/C9NR01118H.
[25] M. Jia, W. Mi, S. Guo, Q.Z. Yang, Y. Jin, N. Shao, Peptide-capped functionalized Ag/Au bimetal nanoclusters with enhanced red fluorescence for lysosome-targeted imaging of hypochlorite in living cells, Talanta 216 (2020) 120926, https://doi.org/10.1016/j.talanta.2020.120926.
[26] A.K. Gaigalas, L. Wang, Measurement of the fluorescence quantum yield using a spectrometer with an integrating sphere detector, J. Res. Natl. Inst. Stand Technol. 113 (2008) 17–28, https://doi.org/10.6028/jres.113.004.
[27] S. Das, A. Sahana, A. Banerjee, S. Lohar, D.A. Safin, M.G. Babashkina, M. Bolte, Y. Garcia, I. Hauli, S.K. Mukhopadhyay, Ratiometric fluorescence sensing and intracellular imaging of Al^{3+} ions driven by an intramolecular excimer formation of a pyrimidine-pyrene scaffold, Dalton Trans. 42 (2013) 4757–4763, https://doi.org/10.1039/C3DT32908A.
[28] S. Sarkar, S. Roy, R.N. Saha, S.S. Panja, Thiophene appended dual fluorescent sensor for detection of Hg^{2+} and cysteamine, J. Fluoresc. 28 (2018) 427–437, https://doi.org/10.1007/s10895-017-2204-1.
[29] Z. Liu, W. He, Z. Guo, Metal coordination in photoluminescent sensing, Chem. Soc. Rev. 42 (2013) 1568–1600, https://doi.org/10.1039/C2CS35363F.
[30] Y. Cao, L. Ding, S. Wang, Y. Liu, J. Fan, W. Hu, P. Liu, Y. Fang, Detection and identification of Cu^{2+} and Hg^{2+} based on the cross-reactive fluorescence responses of a dansyl-functionalized film in different solvents, ACS Appl. Mater. Interfaces 6 (2014) 49–56, https://doi.org/10.1021/am405157k.
[31] Z. Zhou, G. Huang, Y. Xiong, M. Zhou, S. Zhang, C.Y. Tang, F.G. Meng, Unveiling the susceptibility of functional groups of poly(ether sulfone)/polyvinylpyrrolidone membranes to NaOCl: a two-dimensional correlation spectroscopic study, Environ. Sci. Technol. 51 (2017) 14342–14351, https://doi.org/10.1021/acs.est.7b03952.

[32] Y.M. Liu, H. Shu, Q.S. Xu, Y.H. Zhang, L.J. Yang, FT-IR study of the SO_2 oxidation behavior in the selective catalytic reduction of NO with NH_3 over commercial catalysts, J. Fuel. Chem. Technol. 43 (2015) 1018–1024, https://doi.org/10.1016/S1872-5813(15) 30030-X.

[33] M.J. Frisch, G.W. Trucks, H.B. Schlegel, G.E. Scuseria, M.A. Robb, J.R. Cheeseman, G. Scalmani, V. Barone, G.A. Petersson, H. Nakatsuji, X. Li, M. Caricato, A.V. Marenich, J. Bloino, B.G. Janesko, R. Gomperts, B. Mennucci, H.P. Hratchian, J.V. Ortiz, A.F. Izmaylov, J.L. Sonnenberg, D. Williams-Young, F. Ding, F. Lipparini, F. Egidi, J. Goings, B. Peng, A. Petrone, T. Henderson, D. Ranasinghe, V.G. Zakrzewski, J. Gao, N. Rega, G. Zheng, W. Liang, M. Hada, M. Ehara, K. Toyota, R. Fukuda, J. Hasegawa, M. Ishida, T. Nakajima, Y. Honda, O. Kitao, H. Nakai, T. Vreven, K. Throssell, J.A.Jr. Montgomery, J.E. Peralta, F. Ogliaro, M.J. Bearpark, J. J. Heyd, E.N. Brothers, K.N. Kudin, V.N. Staroverov, T.A. Keith, R. Kobayashi, J. Normand, K. Raghavachari, A.P. Rendell, J.C. Burant, S.S. Iyengar, J. Tomasi, M. Cossi, J.M. Millam, M. Klene, C. Adamo, R. Cammi, J.W. Ochterski, R.L. Martin, K. Morokuma, O. Farkas, J.B. Foresman, D.J. Fox, Gaussian, Inc., Wallingford CT, 2016.

[34] A.D. Becke, Density-functional thermochemistry. III. The role of exact exchange, J. Chem. Phys. 98 (1993) 5648–5652, https://doi.org/10.1063/1.464913.